Machine Intelligence & Robotic Control, Vol. 5, No. 2, 33–44 (2003)

Paper

Position/Force Control of a Walking Robot*

Manuel F. Silva†, J. A. Tenreiro Machado†, and António M. Lopes‡

Abstract: This paper analyzes the performance of a classical position *PD* algorithm and a new cascade controller, involving position and force feedback loops, for multi-legged locomotion systems. For that objective the robot prescribed motion is characterized in terms of several locomotion variables. A group of indices measures the walking performance based on the robot and terrain dynamical properties and on the robot hip trajectories. A set of experiments reveals the performance of the control architectures in the viewpoint of the proposed indices.

Keywords: Walking Robots, Control Algorithms, *PID* Control Algorithm, Cascade Control

1. Introduction

WALKING machines allow locomotion in terrain inaccessible to other type of vehicles, since they do not need a continuous support surface [1]. On the other hand, the requirements for leg coordination and control impose difficulties beyond those encountered in wheeled robots [2]. There exists a class of walking machines for which walking is a natural dynamic mode. Once started on a shallow slope, a machine of this class will settle into a steady gait, without active control or energy input [3], [4]. However, the capabilities of these machines are quite limited. Previous studies focused mainly in the control at the leg level and leg coordination using neural networks [5], [6], fuzzy logic [7], central pattern generators [8], [9] and subsumption architecture [10], [11]. There is also a growing interest in using insect locomotion schemes to control walking robots [12]–[15]. In spite of the diversity of approaches, for multi-legged robots the control at the joint level is usually implemented through a simple *PID* scheme with position/velocity feedback [9], [14]. Other approaches include sliding mode control [16], computed torque control [17], hybrid force/position control [18] and fractional order control [19].

With these facts in mind, a simulation model for multi-leg locomotion systems was developed, for several periodic gaits. Based on this tool, the present study compares two different robot control architectures, namely a Proportional-Derivative position algorithm (*PD-P*) and a cascade of a Proportional-Derivative position control with foot force feedback (*PD-P&F*). For the case of the *PD-P&F* it is also implemented an adjusting scheme that varies the gain in the forward force loop according with the step evolution.

The aim of the study is to verify the performance of the two control architectures and the influence of foot force feedback on the system stability and robustness for variable ground characteristics. In this line of thought, the analysis is based on the formulation of a set of indices measuring the robot and ground dynamics as well as the hip trajectory errors during walking.

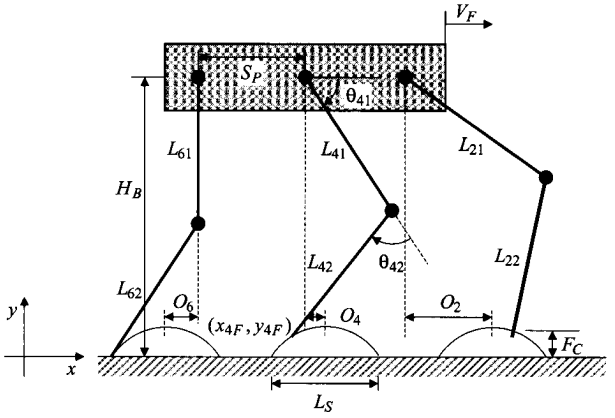

Fig. 1 Coordinate system and variables that characterize the motion trajectories of the multi-legged robot

Several simulations reveal the superior performance of the control architecture with foot force feedback and a gain-adjusting scheme of the forward force loop during the support phase. This control algorithm minimizes the proposed indices, particularly in real situations where we have non-ideal actuators with saturation.

Bearing these facts in mind, the paper is organized as follows. Section 2 introduces the hexapod model and the motion-planning scheme. Sections 3 and 4 present the robot control architecture and formulate the optimizing indices, respectively. After this, Section 5 develops a set of experiments that reveal the performance of the different control architectures and, finally, Section 6 outlines the main conclusions. This paper concludes with an appendix, in Section 7, describing the ground model and the parameter calculation.

2. Robot Kinematics and Trajectory Planning

We consider a walking system with n legs, equally distributed along both sides of the robot body, having each one two rotational joints (**Fig. 1**).

Motion is described by means of a world coordinate sys-

* Received July 31, 2003; accepted January 8, 2004.

† Department of Electrical Engineering, Institute of Engineering of Porto, Rua Dr. António Bernardino de Almeida, 4200-072 Porto, Portugal. Email: {mfsilva,jtm}@dee.isep.ipp.pt

‡ Department of Mechanical Engineering, Faculty of Engineering of Porto, Rua Dr. Roberto Frias, 4200-065 Porto, Portugal. Email: aml@fe.up.pt

tem. The kinematic model comprises: the cycle time T, the duty factor β, the transference time $t_T = (1-\beta)T$, the support time $t_S = \beta T$, the step length L_S, the stroke pitch S_P, the body height H_B, the maximum foot clearance F_C, the ith leg lengths L_{i1} and L_{i2} and the foot trajectory offset O_i ($i = 1, \ldots, n$). Moreover, we consider a periodic trajectory for each foot, with body velocity $V_F = L_S/T$.

Given a particular gait and duty factor β, it is possible to calculate for leg i the corresponding phase ϕ_i and the time instant where each leg leaves and returns to contact with the ground [2].

From these results, and knowing T, β and t_S, the Cartesian trajectories of the tip of the feet must be completed during t_T. Based on this data, the trajectory generator is responsible for producing a motion that synchronizes and coordinates the legs.

For each cycle the desired trajectory of the foot of the swing leg is computed either through cycloidal (Eq. (1)) or sinusoidal (Eq. (2)) functions. For example, considering that the transfer phase starts at $t = 0$ s, for leg $i = 1$ we have the foot trajectory $\boldsymbol{p}_{Fd}(t) = [x_{iFd}(t) \;\; y_{iFd}(t)]^T$:

- during the transfer phase:

$$\boldsymbol{p}_{Fd}(t) = \begin{bmatrix} V_F \left[t - \dfrac{1}{2\pi f} \sin\left(\dfrac{2\pi t}{T}\right)\right] \\ \dfrac{F_C}{2}\left[1 - \cos\left(\dfrac{2\pi t}{T}\right)\right] \end{bmatrix} \quad (1)$$

$$\boldsymbol{p}_{Fd}(t) = \begin{bmatrix} \left(\dfrac{t_T}{T}\right)\left[\left(\dfrac{L_S t}{t_T}\right) - \dfrac{L_S}{2\pi}\sin\left(\dfrac{2\pi t}{T}\right)\right] \\ \dfrac{2F_C t'}{T} - \dfrac{F_C}{2\pi}\sin\left(\dfrac{4\pi t'}{T}\right) \end{bmatrix},$$

$$t' = \begin{cases} t, & 0 \le t < T/2 \\ T - t, & T/2 \le t < T \end{cases} \quad (2)$$

- during the stance phase:

$$\boldsymbol{p}_{Fd}(t) = [V_F T \quad 0]^T. \quad (3)$$

The robot body, and by consequence the legs hips, is assumed to have a desired horizontal movement with a constant forward speed V_F. Therefore, for leg i the Cartesian coordinates of the hip of the legs are given by $\boldsymbol{p}_{Hd}(t) = [x_{iHd}(t) \;\; y_{iHd}(t)]^T$:

$$\boldsymbol{p}_{Hd}(t) = [V_F t \quad H_B]^T. \quad (4)$$

Once defined the coordinates of the feet and hips of the robot it is possible to obtain the leg joint positions and velocities using the inverse kinematics ψ^{-1} and the Jacobian $\boldsymbol{J} = \partial\psi/\partial\boldsymbol{q}$.

The algorithm for the forward motion planning accepts the desired Cartesian trajectories of the legs feet $\boldsymbol{p}_{Fd}(t)$ and hips $\boldsymbol{p}_{Hd}(t)$ as inputs and, by means of an inverse kinematics algorithm, generates the related joint trajectories $\boldsymbol{q}_d(t) = [\theta_{i1d}(t) \;\; \theta_{i2d}(t)]^T$, selecting the solution corresponding to a forward knee:

$$\boldsymbol{p}_d(t) = [x_{id}(t) \quad y_{id}(t)]^T = \boldsymbol{p}_{Hd}(t) - \boldsymbol{p}_{Fd}(t) \quad (5)$$

$$\boldsymbol{p}_d(t) = \boldsymbol{\psi}[\boldsymbol{q}_d(t)] \Rightarrow \boldsymbol{q}_d(t) = \boldsymbol{\psi}^{-1}[\boldsymbol{p}_d(t)] \quad (6)$$

$$\dot{\boldsymbol{q}}_d(t) = \boldsymbol{J}^{-1}[\dot{\boldsymbol{p}}_d(t)]. \quad (7)$$

In order to avoid the impact and friction effects, at the planning phase we estimate null velocities of the feet in the instants of landing and taking off, assuring also the velocity continuity.

3. Robot Dynamics and Control Architecture

The planned joint trajectories constitute the reference for the robot control system. The model for the robot inverse dynamics is formulated as:

$$\boldsymbol{\Gamma} = \boldsymbol{H}(\boldsymbol{q})\ddot{\boldsymbol{q}} + \boldsymbol{c}(\boldsymbol{q}, \dot{\boldsymbol{q}}) + \boldsymbol{g}(\boldsymbol{q}) - \boldsymbol{F}_{RH} - \boldsymbol{J}_F^T(\boldsymbol{q})\boldsymbol{F}_{RF} \quad (8)$$

where $\boldsymbol{\Gamma} = [f_{ix} \;\; f_{iy} \;\; \tau_{i1} \;\; \tau_{i2}]^T$ ($i = 1, \ldots, n$) is the vector of forces/torques, $\boldsymbol{q} = [x_{iH} \;\; y_{iH} \;\; \theta_{i1} \;\; \theta_{i2}]^T$ is the vector of position coordinates, $\boldsymbol{H}(\boldsymbol{q})$ is the inertia matrix and $\boldsymbol{c}(\boldsymbol{q}, \dot{\boldsymbol{q}})$ and $\boldsymbol{g}(\boldsymbol{q})$ are the vectors of centrifugal/Coriolis and gravitational forces/torques, respectively. The $n \times m$ matrix $\boldsymbol{J}_F^T(\boldsymbol{q})$ is the transpose of the robot Jacobian matrix, $\boldsymbol{F}_{RH}$ is the $m \times 1$ vector of the body inter-segment forces and $\boldsymbol{F}_{RF}$ is the $m \times 1$ vector of the reaction forces that the ground exerts on the robot feet. Concerning $\boldsymbol{F}_{RF}$, it is considered that these forces are null during the foot transfer phase.

During the system simulation, Eq. (8) is integrated through the Runge-Kutta method [20].

Furthermore, we consider that the joint actuators are not ideal, exhibiting a saturation given by:

$$\tau_{ijm} = \begin{cases} \tau_{ijC}, & |\tau_{ijm}| \le \tau_{ijMax} \\ \mathrm{sgn}(\tau_{ijC})\tau_{ijMax}, & |\tau_{ijm}| > \tau_{ijMax} \end{cases} \quad (9)$$

where, for leg i and joint j, τ_{ijC} is the controller demanded torque, τ_{ijMax} is the maximum torque that the actuator can supply and τ_{ijm} is the motor effective torque.

Figure 2 presents the dynamic model for the hexapod body and foot-ground interaction.

The contact of the ith robot feet with the ground is modeled through a non-linear system [21] with damping $B'_{\eta F}$ and stiffness $K_{\eta F}$ ($\eta = \{x, y\}$) in the {horizontal, vertical} directions, respectively, according with the equations:

$$f_{ixF} = -K_{xF}\Delta_{ixF} - B'_{xF}\left(-\Delta_{iyF}\right)\dot{\Delta}_{ixF}, \quad \Delta_{ixF} = x_{iF} - x_{iF0}, \quad \dot{\Delta}_{ixF} = \dot{x}_{iF} - \dot{x}_{iF0} \quad (10)$$

$$f_{iyF} = -K_{yF}\Delta_{iyF} - B'_{yF}\left(-\Delta_{iyF}\right)^v \dot{\Delta}_{iyF}, \quad \Delta_{iyF} = y_{iF} - y_{iF0}, \quad \dot{\Delta}_{iyF} = \dot{y}_{iF} - \dot{y}_{iF0} \quad (11)$$

where x_{iF0} and y_{iF0} are the coordinates of foot i touchdown and $v \approx 1.0$ is a parameter dependent on the ground characteristics [22].

Furthermore, the robot body is divided in n identical segments (each with mass $M_b n^{-1}$) and a linear spring-dashpot

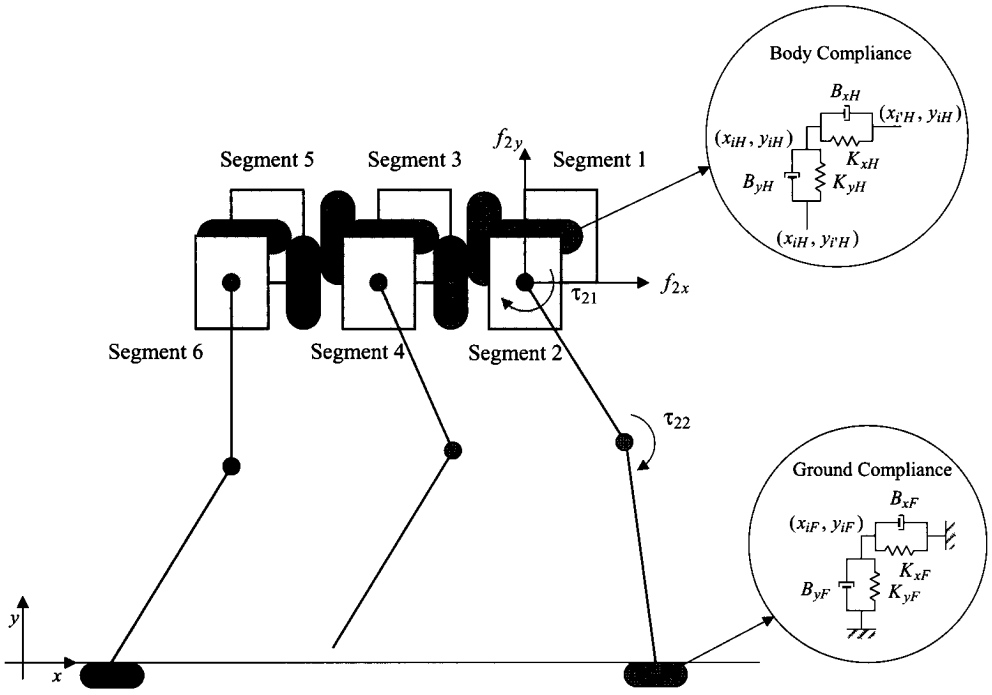

Fig. 2 Model of the robot body and foot-ground interaction

system is adopted to implement the intra-body compliance:

$$f_{ixH} = \sum_{i'=1}^{u} \left(-K_{xH}\Delta_{i'xH} - B_{xH}\dot{\Delta}_{i'xH} \right), \quad (12)$$
$$\Delta_{i'xH} = x_{iH} - x_{i'H}, \quad \dot{\Delta}_{i'xH} = \dot{x}_{iH} - \dot{x}_{i'H}$$

$$f_{iyH} = \sum_{i'=1}^{u} \left(-K_{yH}\Delta_{i'yH} - B_{yH}\dot{\Delta}_{i'yH} \right), \quad (13)$$
$$\Delta_{i'yH} = y_{iH} - y_{i'H}, \quad \dot{\Delta}_{i'yH} = \dot{y}_{iH} - \dot{y}_{i'H}$$

where $(x_{i'H}, y_{i'H})$ are the hip coordinates and u is the total number of segments adjacent to leg i, respectively.

The general control architecture of the hexapod robot is presented in **Fig. 3**. The trajectory planning is held at the Cartesian space but the control is performed in the joint space, which requires the integration of the inverse kinematic model in the forward path. The base algorithm (*PD-P*) considers only a position/velocity feedback and, consequently, the series of G_{c1} and G_{c2} can be substituted by a single block. The base architecture is improved with the introduction of a second internal feedback loop with information of the foot-ground interaction force (*PD-P&F*). In this case, G_{c1} and G_{c2} are in a cascade structure in the forward control path.

For the controller $G_{c1}(s)$ we adopt a position/velocity *PD* algorithm:

$$G_{C1j}(s) = Kp_j + Kd_j s, \quad j = 1, 2 \quad (14)$$

where Kp_j and Kd_j are the proportional and derivative gains for joint j, respectively.

For G_{c2} we consider a simple P controller with gain Kp_j that is varied according to a scheme described in the sequel.

4. Measures for Performance Evaluation

In mathematical terms we establish four global measures of the overall performance of the mechanism in an average sense [23]–[25]. In this perspective, we define three indices $\{E_{av}, F_L, \tau_P\}$ inspired on the robot dynamics and one index $\{\varepsilon_{xyH}\}$ based on the hip trajectory tracking errors.

A first measure in this analysis is the mean absolute density of energy per traveled distance. This index is computed assuming that energy regeneration is not available by actuators doing negative work, that is, by taking the absolute value of the power. At a given joint j (each leg has $m = 2$ joints) and leg i (since we are adopting an hexapod it yields $n = 6$ legs), the mechanical power is the product of the motor torque and angular velocity. The global index E_{av} is obtained by averaging the mechanical absolute energy delivered over the traveled distance L:

$$E_{av} = \frac{1}{L} \sum_{i=1}^{n} \sum_{j=1}^{m} \int_0^T \left| \tau_{ijm}(t)\dot{\theta}_{ij}(t) \right| dt. \quad (15)$$

A second measure is the index F_L that considers the forces that occur on the hips of the robot per traveled distance L:

$$F_L = \frac{1}{L} \sqrt{\sum_{i=1}^{n} \int_0^T \left\{ [f_{ix}(t)]^2 + [f_{iy}(t)]^2 \right\} dt}. \quad (16)$$

Since the two previous indices capture, mainly, the low frequency system behavior we define the index τ_P that measures the robot torque peaks demanded by the controller when responding to high frequency phenomena, such as foot-ground impacts:

$$\tau_P = \max \left| \tau_{ijC}(t) \right|. \quad (17)$$

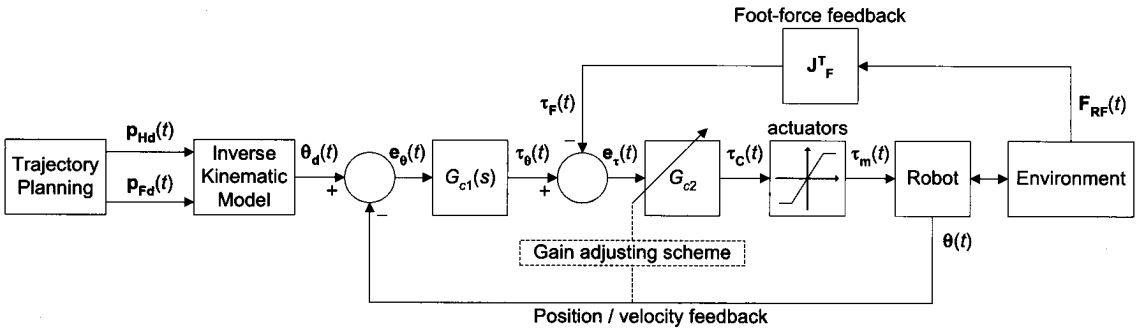

Fig. 3 Hexapod robot control architecture

Table 1 Locomotion parameters

β	50%
L_S	1 m
H_B	0.9 m
F_C	0.1 m
V_F	1 ms^{-1}

Table 2 Robot model parameters

S_P	1 m
L_{ij}	0.5 m
O_i	0 m
M_{ij}	1 kg
M_b	88.0 kg
M_{if}	0.0 kg
K_{xH}	10^5 Nm^{-1}
K_{yH}	10^4 Nm^{-1}
B_{xH}	10^3 Nsm^{-1}
B_{yH}	10^2 Nsm^{-1}

Table 3 Ground parameters

K_{xF}	1302152 Nm^{-1}
K_{yF}	1705199 Nm^{-1}
B'_{xF}	2364932 Nsm^{-1}
B'_{yF}	2706233 Nsm^{-1}
v	0.9

In what concerns the hip trajectory following errors we can define the index:

$$\varepsilon_{xyH} = \sum_{i=1}^{n} \sqrt{\frac{1}{N_S} \sum_{k=1}^{N_S} \left(\Delta_{ixH}^2 + \Delta_{iyH}^2\right)},$$
$$\Delta_{ixH} = x_{iH}^d(k) - x_{iH}^r(k), \tag{18}$$
$$\Delta_{iyH} = y_{iH}^d(k) - y_{iH}^r(k)$$

where N_S is the total number of samples for averaging purposes and $\{d, r\}$ indicate the ith samples of the desired and real position, respectively.

In all cases the performance optimization requires the minimization of each index.

5. Simulation Results

In this section we develop a set of simulations to compare the controller performances during a periodic Wave gait, while the robot is considered to be traversing a perfectly horizontal surface.

In case of locomotion in terrains with obstacles, the robot should adapt its gait to the environment. If the number of obstacles is small, the locomotion can be accomplished using a quasi periodic gait, for which the trajectory planning using the algorithms described in [26] can be used. In case of more rugged terrains, other planning algorithms are available [27]–[29].

5.1 System parameters and controller tuning

For simulation purposes we consider the locomotion parameters, the robot body parameters and the ground parameters (considering that the ground is of compact clay—see Appendix) presented in **Tables 1, 2 and 3**, respectively.

To tune the controller parameters we adopt a systematic method, testing and evaluating several possible combinations of controller parameters, for both architectures. Moreover, it is assumed high performance joint actuators with a maximum actuator torque in Eq. (9) of τ_{ijMax} = 400 Nm.

Table 4 Controller parameters for $G_{c1}(s)$ and G_{c2} when minimizing the hips trajectories errors ε_{xyH}

PD-P	$G_{c1}(s)$	Joint j = 1	Kp_{i1}	1000
			Kd_{i1}	100
		Joint j = 2	Kp_{i2}	4500
			Kd_{i2}	20
	$G_{c2}(s)$	Joint j = 1	Kp_{i1}	1.0
		Joint j = 2	Kp_{i2}	1.0
PD-P&F	$G_{c1}(s)$	Joint j = 1	Kp_{i1}	1000
			Kd_{i1}	100
		Joint j = 2	Kp_{i2}	4500
			Kd_{i2}	20
	$G_{c2}(s)$	Joint j = 1	Kp_{i1}	0.9
		Joint j = 2	Kp_{i2}	0.9

The minimization of the hips trajectories errors (ε_{xyH}) leads to the $G_{c1}(s)$ and G_{c2} controller parameters presented in **Table 4**.

Through the analysis of the plots of **Figs. 4** and **5** we conclude that the *PD-P&F* control architecture improves the

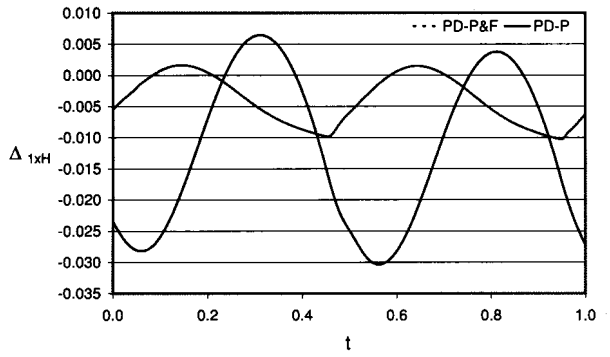

Fig. 4 Plots of the hip trajectory error Δ_{1xH} *vs.* t for the *PD-P* and the *PD-P&F* control architectures, with $\tau_{ijMax} = 400$ Nm

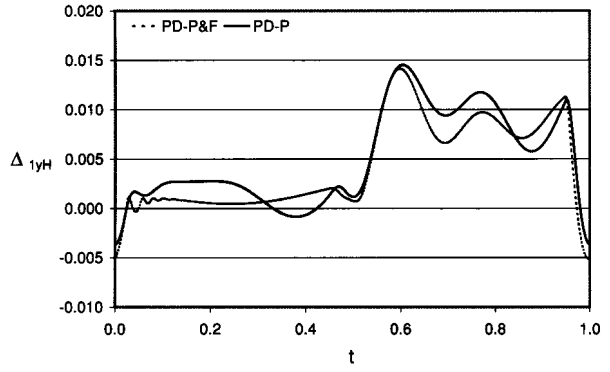

Fig. 5 Plots of the hip trajectory error Δ_{1yH} *vs.* t for the *PD-P* and the *PD-P&F* control architectures, with $\tau_{ijMax} = 400$ Nm

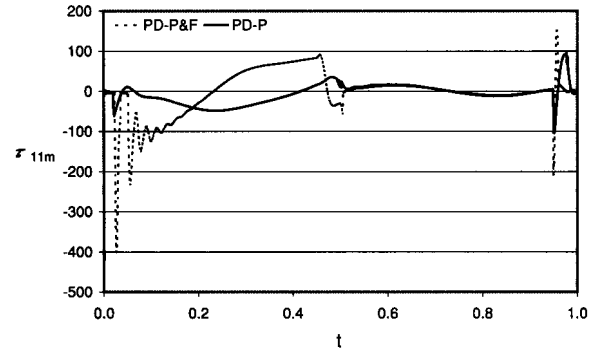

Fig. 6 Plots of the joint torque τ_{11m} *vs.* t for the *PD-P* and the *PD-P&F* control architectures, with $\tau_{ijMax} = 400$ Nm

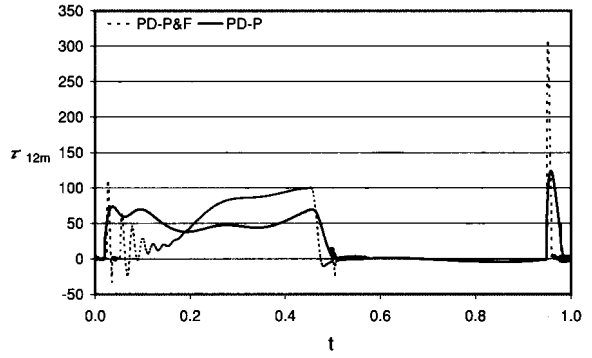

Fig. 7 Plots of the joint torque τ_{12m} *vs.* t for the *PD-P* and the *PD-P&F* control architectures, with $\tau_{ijMax} = 400$ Nm

Table 5 Controller parameters for $G_{c1}(s)$ and G_{c2} when establishing a compromise between the minimization of E_{av} and ε_{xyH}

PD-P	$G_{c1}(s)$	Joint $j = 1$	Kp_{i1}	2000
			Kd_{i1}	0
		Joint $j = 2$	Kp_{i2}	2500
			Kd_{i2}	60
	$G_{c2}(s)$	Joint $j = 1$	Kp_{i1}	1.0
		Joint $j = 2$	Kp_{i2}	1.0
PD-P&F	$G_{c1}(s)$	Joint $j = 1$	Kp_{i1}	8000
			Kd_{i1}	60
		Joint $j = 2$	Kp_{i2}	500
			Kd_{i2}	40
	$G_{c2}(s)$	Joint $j = 1$	Kp_{i1}	0.9
		Joint $j = 2$	Kp_{i2}	0.9

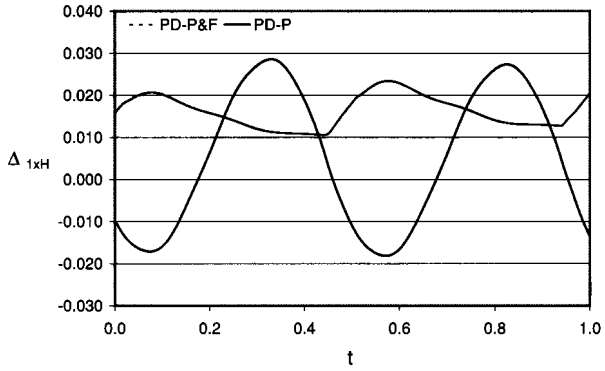

Fig. 8 Plots of the hip trajectory error Δ_{1xH} *vs.* t for the *PD-P* and the *PD-P&F* control architectures, with $\tau_{ijMax} = 400$ Nm

hip trajectory tracking (and presents a lower value for the index ε_{xyH}) but at the cost of larger joint driving torques (**Figs. 6** and **7**) and higher values of E_{av}, F_L and τ_P.

In order to make a proper comparison of both controllers, namely with the variation of the locomotion and the environment parameters, we establish a compromise in what concerns the minimization of E_{av} and ε_{xyH}. Therefore, we adopt the $G_{c1}(s)$ parameters presented in **Table 5** and we maintain the value of the proportional controller G_{c2} gain Kp_j.

For this new set of controller parameters we conclude again that the *PD-P&F* improves the hip trajectory tracking (**Figs. 8** and **9**), while presenting similar joint torques (**Figs. 10** and **11**) to the *PD-P*. Furthermore, in the case of the *PD-P* the joint torque τ_{12m} presents a considerable oscillation at the instants of feet impact in the ground (which occur around $t = 0.5$ s) and a more subtle oscillation during the foot support phase ($0.5\text{ s} < t < 1.0\text{ s}$).

5.2 Foot trajectory and actuator saturation

With the robot, ground and controller parameters of Tables 1–3 and 5 we evaluate the two alternative foot transfer trajectories $\boldsymbol{p}_{Fd}(t)$, namely the cycloidal and the sinusoidal functions, presented in Eqs. (1) and (2). From **Figs. 12** and **13** it is possible to conclude that the cycloidal foot transfer function is superior because it improves the hip tra-

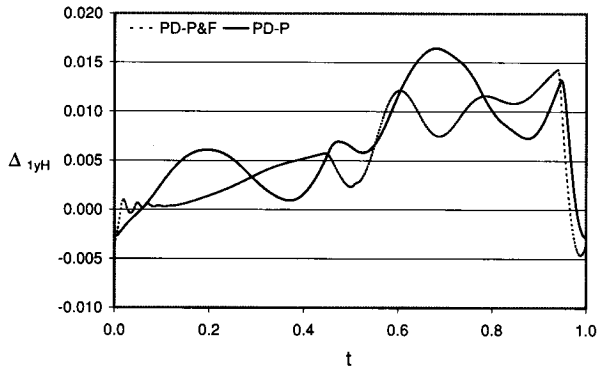

Fig. 9 Plots of the hip trajectory error Δ_{1yH} *vs.* t for the *PD-P* and the *PD-P&F* control architectures, with $\tau_{ijMax} = 400$ Nm

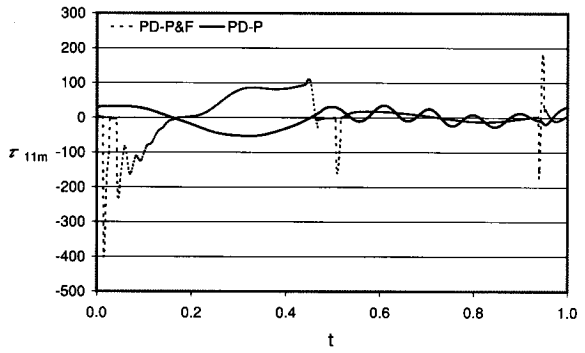

Fig. 10 Plots of the joint torque τ_{11m} *vs.* t for the *PD-P* and the *PD-P&F* control architectures, with $\tau_{ijMax} = 400$ Nm

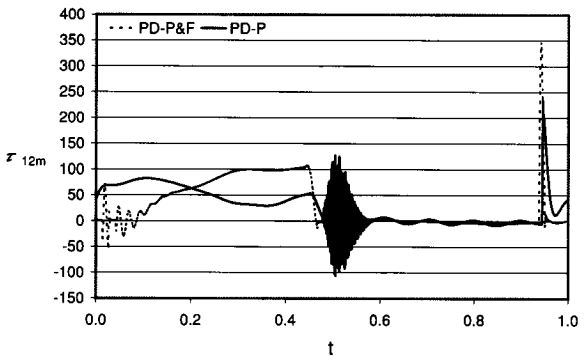

Fig. 11 Plots of the joint torque τ_{12m} *vs.* t for the *PD-P* and the *PD-P&F* control architectures, with $\tau_{ijMax} = 400$ Nm

jectory tracking, while minimizing the corresponding joint torques. Furthermore, in the case of the sinusoidal foot transfer trajectory, the joint torques present large amplitude spikes in the instants of feet take-off and landing, which can be observed for τ_{11m} around $t = 0$, 0.5 and 1.0 s in **Fig. 13**. These spikes are due to some dragging of the feet on the ground caused by the shape of the sinusoidal function. For different acceleration profiles of the foot trajectory there were no significant changes of these charts. Based on this conclusion, in the sequel we adopt only the cycloidal foot trajectory when testing the control algorithms.

Another important aspect is the required actuator action. Therefore, we decide to test both controller performances when varying the level of actuator saturation (τ_{ijMax}). The *PD-P&F* controller architecture presents lower values of

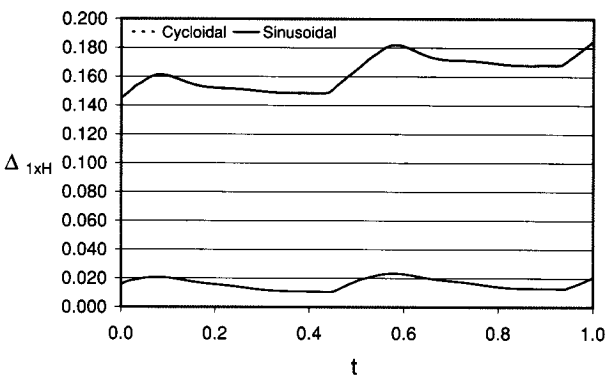

Fig. 12 Plots of the hip trajectory error $\Delta_{1xH}(t)$ for the *cycloidal* and *sinusoidal* feet trajectories, with the *PD-P&F* controller and $\tau_{ijMax} = 400$ Nm

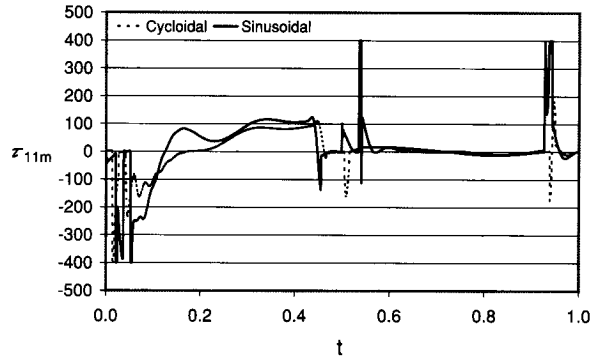

Fig. 13 Plots of the joint torque $\tau_{11m}(t)$ for the *cycloidal* and *sinusoidal* feet trajectories, with the *PD-P&F* controller and $\tau_{ijMax} = 400$ Nm

ε_{xyH} for values of $\tau_{ijMax} > 100$ Nm. On the other hand, both controllers present similar values of E_{av} in this interval. In the case of strong actuator saturation level ($\tau_{ijMax} < 100$ Nm) the two algorithms have difficulties in controlling the robot locomotion and, as a consequence, the values of the indices ε_{xyH} and E_{av} increase sharply, being this effect slightly higher in the case of the *PD-P&F* controller.

During the feet collisions with the ground, at the instants of feet landing, high contact forces occur that propagate through the robot legs, leading to large values of the index F_L. Moreover, those contact forces feed-back in the controller force loop leading to large values of the index τ_P, for the *PD-P&F* scheme. For this reason, the *PD-P* controller architecture presents lower values for the indices F_L and τ_P for the entire range of τ_{ijMax}.

5.3 Locomotion parameters

An important aspect that must be investigated is the influence of the locomotion parameters. Therefore, we test the two control architectures for variations of the duty factor β, the robot forward locomotion velocity V_F and the locomotion gait.

The duty factor was varied within the interval capable of achieving a stable locomotion ($20\% \leq \beta \leq 80\%$). The four indices are lower in the case of the *PD-P&F* architecture, for all values of τ_{ijMax}.

Regarding the variation of the robot velocity, the results were analyzed for $0.5\ \text{ms}^{-1} < V_F < 6.0\ \text{ms}^{-1}$.

For the entire range of variation of V_F, the *PD-P&F* control scheme presents the lower values for ε_{xyH}. Concerning the dynamical indices, for $\tau_{ijMax} > 100$ Nm, their behaviour is similar and we have superior performances for the *PD-P&F* scheme if $V_F < 1.0\ \text{ms}^{-1}$ or $V_F > 3.0\ \text{ms}^{-1}$ and for the *PD-P* architecture if $1.0\ \text{ms}^{-1} < V_F < 3.0\ \text{ms}^{-1}$.

In what concerns the locomotion parameters, we finally tested the controllers performance under different locomotion gaits, namely with Equal Phase Half Cycle, Equal Phase Full Cycle, Backward Wave, Backward Equal Phase Half Cycle and Backward Equal Phase Full Cycle [2], for values of the duty factor capable of achieving a stable locomotion ($20\% \leq \beta \leq 80\%$). The results show that, for both control schemes, the best performance is attained for the Wave gait, being the results quite similar to the Backward Wave gait. Concerning the other four gaits, the performance indices are similar for all of them.

5.4 Ground properties

Based on the experiments presented previously we examine both control architectures for distinct ground properties. Therefore, in a first phase we start by considering the *PD-P* controller and different values of (K_{xF}, K_{yF}, B_{xF}, B_{yF}), in order to observe its influence upon the proposed indices, for actuators such that $\tau_{ijMax} = 400$ Nm. In a second phase we repeat the experiments for the case of a *PD-P&F* control architecture.

The range of ground model parameters allow us to simulate the behavior of the ground from peat to gravel. For ground parameters similar to those of concrete and wood, both algorithms present difficulties in controlling the robot locomotion with the adopted parameters, due to the impacts that appear during the feet landing. In this case there are two options: we can find another tuning for the controllers or we can equip the robot feet with some shock absorbing device [30]–[33].

The performance measures *versus* the multiplying coefficient of ground parameters, with relation to base experiment, are presented in **Figs. 14–17**. We conclude that the robot hips trajectories errors (measured through the index ε_{xyH}) are smaller when we adopt a *PD-P&F* control architecture, for values of the ground parameters below those adopted in the base experience (soft grounds) and above $4\times$ the base parameter values (hard soils), for which case the *PD-P* control architecture finds problems in correctly controlling the system.

The behavior of the index E_{av} is similar to ε_{xyH}. Concerning the indices F_L and τ_P they are higher in the case of the *PD-P&F* control architecture for all types of ground.

For moderate levels of actuator saturation (e.g., $\tau_{ijMax} = 150$ Nm), we get similar conclusions.

In the case of strong actuator saturation (e.g., $\tau_{ijMax} < 140$ Nm) the indices reveal a large performance degradation with difficulties both for the *PD-P&F* and the *PD-P* controllers. Nevertheless, this situation is not realistic since it corresponds to operating conditions requiring joint torques much higher than those established by the saturation level. On the other hand, when we have high performance actuators ($\tau_{ijMax} > 400$ Nm), the *PD-P&F* scheme reveals stability problems, particularly on hard terrains (values of the ground parameters above 100% of the base values) due to the impulses of force feedback during the impacts of the feet with the ground (**Figs. 18** and **19**).

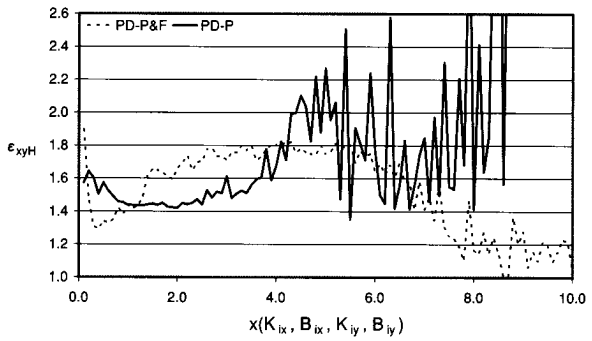

Fig. 14 Plot of ε_{xyH} *vs.* $\times(K_{xF}, K_{yF}, B_{xF}, B_{yF})$ for the *PD-P* and the *PD-P&F* control architectures, with $\tau_{ijMax} = 400$ Nm

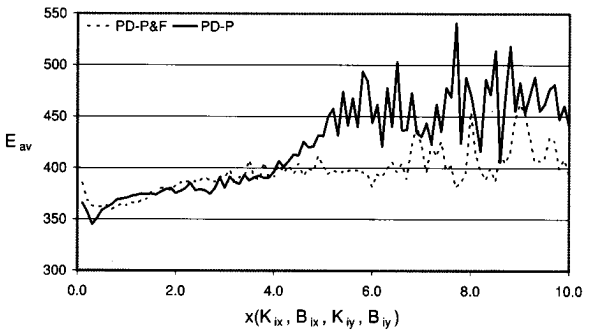

Fig. 15 Plot of E_{av} *vs.* $\times(K_{xF}, K_{yF}, B_{xF}, B_{yF})$ for the *PD-P* and the *PD-P&F* control architectures, with $\tau_{ijMax} = 400$ Nm

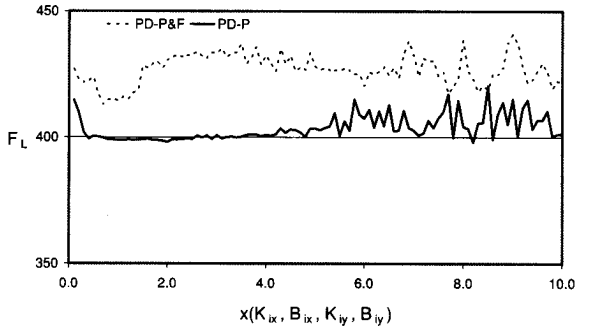

Fig. 16 Plot of F_L *vs.* $\times(K_{xF}, K_{yF}, B_{xF}, B_{yF})$ for the *PD-P* and the *PD-P&F* control architectures, with $\tau_{ijMax} = 400$ Nm

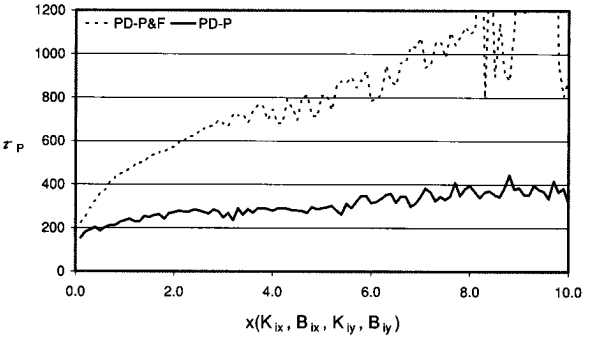

Fig. 17 Plot of τ_P *vs.* $\times(K_{xF}, K_{yF}, B_{xF}, B_{yF})$ for the *PD-P* and the *PD-P&F* control architectures, with $\tau_{ijMax} = 400$ Nm

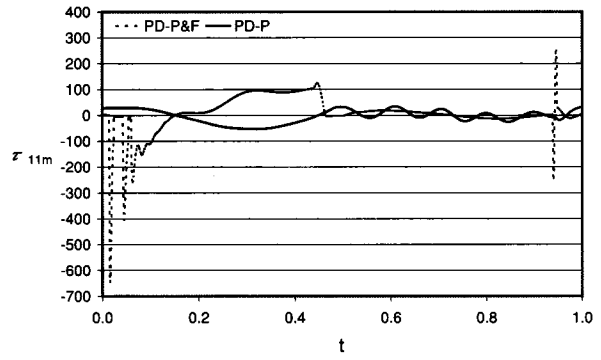

Fig. 18 Plots of the of the joint torque τ_{11m} *vs.* t for the *PD-P* and the *PD-P&F* control architectures, with $\tau_{ijMax} \rightarrow \infty$

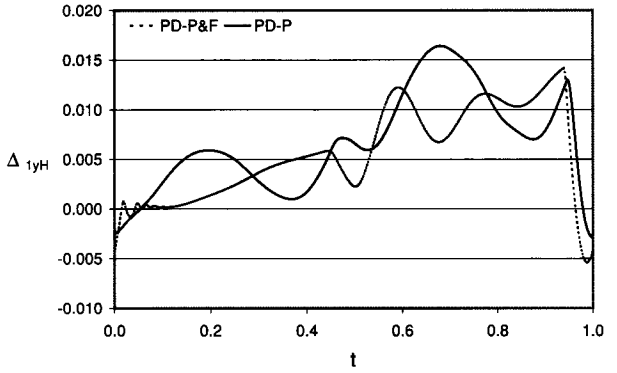

Fig. 19 Plots of the hip trajectory error Δ_{1yH} *vs.* t for the *PD-P* and the *PD-P&F* control architectures, with $\tau_{ijMax} \rightarrow \infty$

However, this case is also not realistic since it assumes ideal actuators exhibiting infinite joint driving torque and infinite bandwidth.

In conclusion, the foot-force feedback seems essential for a robust control performance during walking in terrain with variable dynamical characteristics.

5.5 Adaptive scheme for the G_{c2} controller gains

An aspect that must be evaluated for the *PD-P&F* scheme is the effect of G_{c2} upon its performance. **Figures 20–22** reveal that a larger proportional gain Kp_j $(j = 1, 2)$ leads to smaller ε_{xyH}, E_{av} and F_L but, on the other hand, degrades the index τ_P (**Fig. 23**). Moreover, high G_{c2} gains lead to large feet-ground impacts that propagate through the control loop up to the actuators, as previously mentioned.

The results point out that the main problem with the *PD-P&F* scheme are the high gains in the forward loop, leading to large feet-ground impacts that propagate through the control loop up to the actuators, at the instants of feet landing.

Bearing these facts in mind, we establish a gain scheduling policy that varies the gain adaptively in accordance with the feet relative position to the ground. The idea is to reduce the proportional gains Kp_j $(j = 1, 2)$, of the G_{c2} controller, before the instants of feet landing and to increase them again after the feet take-off.

Figures 24–27 depict the four indices *versus* the value of the gains Kp_j of the G_{c2} controller when the feet are in the

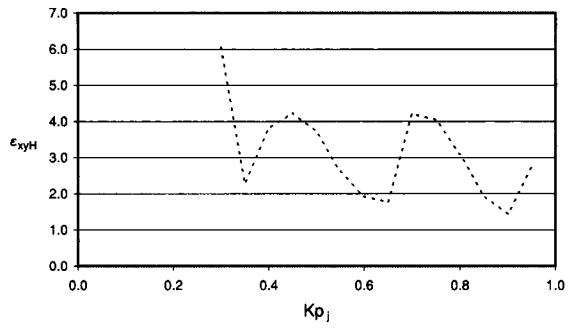

Fig. 20 Plot of ε_{xyH} *vs.* Kp_j for the *PD-P&F* controller, with $\tau_{ijMax} = 400$ Nm

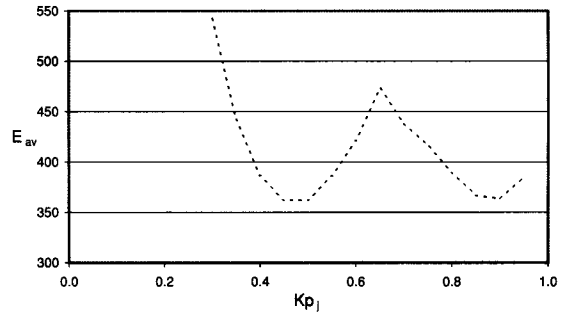

Fig. 21 Plot of E_{av} *vs.* Kp_j for the *PD-P&F* controller, with $\tau_{ijMax} = 400$ Nm

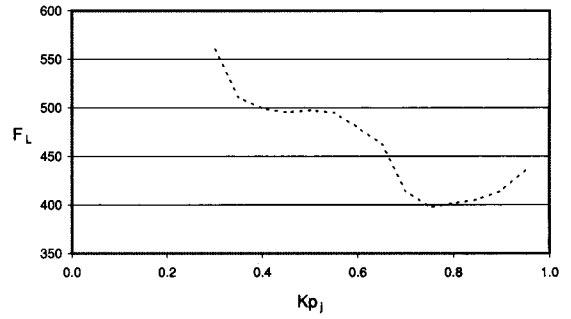

Fig. 22 Plots of F_L *vs.* Kp_j for the *PD-P&F* controller, with $\tau_{ijMax} = 400$ Nm

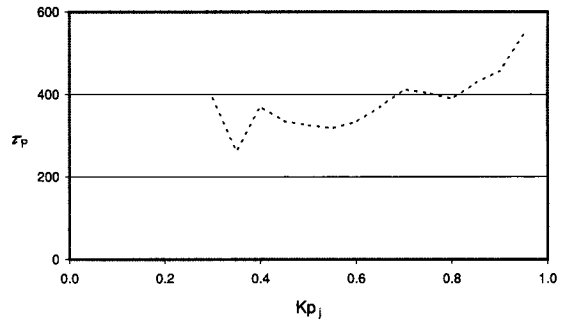

Fig. 23 Plot of τ_P *vs.* Kp_j for the *PD-P&F* controller, with $\tau_{ijMax} = 400$ Nm

support phase (Kp_{jlow}). During the feet transfer phase the value of these gains is $Kp_{jhigh} = 0.9$. The switching between the support and transfer phases is established when

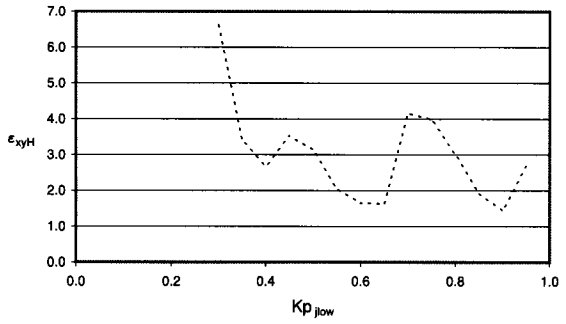

Fig. 24 Plot of ε_{xyH} *vs.* Kp_{jlow} for $\{Kp_{jhigh}, y_{iF0}\} = \{0.9,\ 0.01\}$, with the *PD-P&F* controller and $\tau_{ijMax} = 400$ Nm

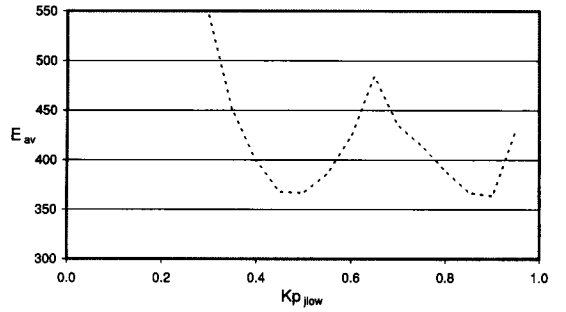

Fig. 25 Plot of E_{av} *vs.* Kp_{jlow} for $\{Kp_{jhigh}, y_{iF0}\} = \{0.9,\ 0.01\}$, with the *PD-P&F* controller and $\tau_{ijMax} = 400$ Nm

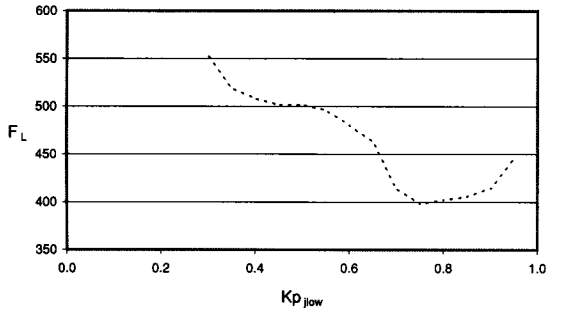

Fig. 26 Plots of F_L *vs.* Kp_{jlow} for $\{Kp_{jhigh}, y_{iF0}\} = \{0.9,\ 0.01\}$, with the *PD-P&F* controller and $\tau_{ijMax} = 400$ Nm

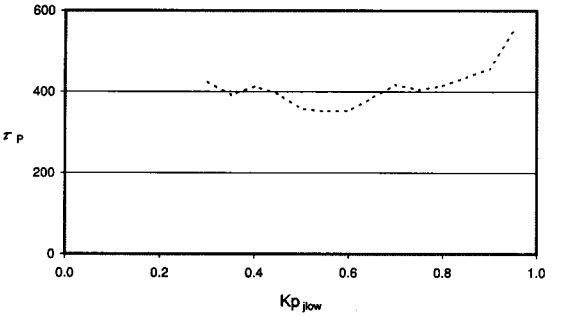

Fig. 27 Plot of τ_P *vs.* Kp_{jlow} for $\{Kp_{jhigh}, y_{iF0}\} = \{0.9,\ 0.01\}$, with the *PD-P&F* controller and $\tau_{ijMax} = 400$ Nm

the distance of the feet to the ground is $y_{iF0} = 0.01$.

Figure 24 reveals that increasing the proportional gain

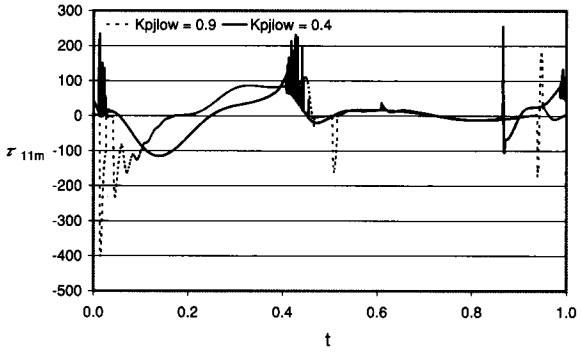

Fig. 28 Plots of the joint torque τ_{11m} *vs.* t for $\{Kp_{jhigh}, y_{iF0}\} = \{0.9,\ 0.01\}$, with the *PD-P&F* controller and $\tau_{ijMax} = 400$ Nm

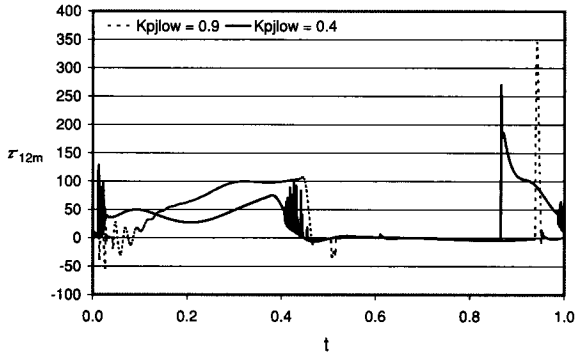

Fig. 29 Plots of the joint torque τ_{12m} *vs.* t for $\{Kp_{jhigh}, y_{iF0}\} = \{0.9,\ 0.01\}$, with the *PD-P&F* controller and $\tau_{ijMax} = 400$ Nm

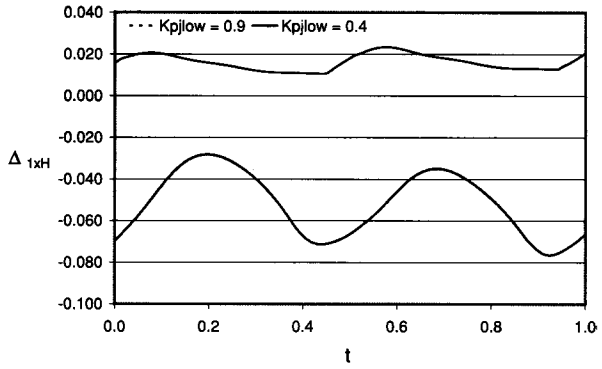

Fig. 30 Plots of the hip trajectory error Δ_{1xH} *vs.* t for $\{Kp_{jhigh}, y_{iF0}\} = \{0.9,\ 0.01\}$, with the *PD-P&F* controller and $\tau_{ijMax} = 400$ Nm

up to $Kp_{jlow} = 0.9$ leads to a better following of the hips trajectories and improves the indices E_{av} and F_L (Figs. 25 and 26, respectively) but, on the other hand, degrade the index τ_P (Fig. 27).

Based on the analysis of these charts, we can find a compromise situation. An adaptive scheme such that $Kp_j(y_{iF}) = Kp_{jlow}$ if $y_{iF} \leq y_{iF0}$ or $Kp_j(y_{iF}) = Kp_{jhigh}$ if $y_{iF} > y_{iF0}$ for $\{Kp_{jlow}, Kp_{jhigh}, y_{iF0}\} = \{0.4,\ 0.9,\ 0.01\}$ leads to a good compromise between the trajectory following errors and the dynamic indices, as can be seen in **Figs. 28–31**.

In conclusion, the foot-force feedback with a reduction

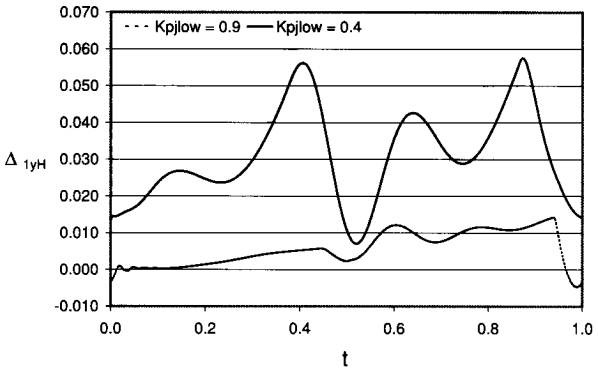

Fig. 31 Plots of the hip trajectory error Δ_{1yH} *vs.* t for $\{Kp_{jhigh}, y_{iF0}\} = \{0.9,\ 0.01\}$, with the *PD-P&F* controller and $\tau_{ijMax} = 400$ Nm

of the proportional gains of the forward loop during the support phase seems essential for establishing a robust control during walking and to accommodate foot-ground interaction phenomena.

6. Conclusions

In this paper we have compared the performance of *PD* control algorithms with position or position and force feedback, in hexapod robots, for different locomotion parameters. Furthermore, we evaluated how the different robot controller architectures respond to non-ideal joint actuators, namely with torque saturation, and variable ground dynamic properties.

For analyzing the system performance four quantitative measures were defined based on the system dynamics and the hip trajectory errors. The experiments reveal that the *PD-P&F* control architecture (cascade controller) is superior to the classical *PD-P* control scheme, from the point of view of the proposed indices. They also show that the cascade controller, with the foot-force feedback and a reduction of the proportional gains of the forward force loop during the support phase, is superior, from the point of view of the proposed indices.

7. Appendix

The contact of the robot feet with the ground can be analyzed through different approaches leading to distinct models. On one hand, it is possible to use the exact force-deflection relationships. On the other hand, and under specific restrictions, it is possible to use approximate models of the ground deformation based on the studies of soil mechanics.

One example of the first approach was used by Manko [1], that models the foot-ground interactions, using force-deflection relationships, for different loading conditions on flat and sloped surfaces. Manko uses a bilinear equation for modeling vertical foot-ground interactions while the lateral forces are modeled with an expression describing an exponential transition to Coulomb's equation. Another example was given by Bekker [34] that relates the vertical sinkage and the local pressure normal to the ground surface though an exponential function. Bekker relates the horizontal deflection with the local shear stress at the ground surface using a quotient of exponential functions.

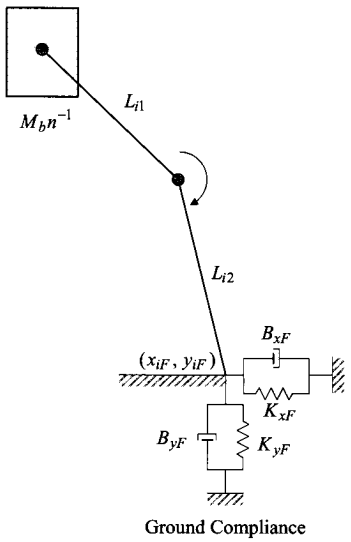

Fig. 32 Mass-Spring-Dashpot model of the foot-ground interaction

The second approach models the foot-ground interaction though a linear system (**Fig. 32**) with damping $B_{\eta F}$ and stiffness $K_{\eta F}$ ($\eta = \{x,\ y\}$) in the {horizontal, vertical} directions, respectively, according to equations [35]:

$$f_{ixF} = -K_{xF}\left(\Delta_{ixF}\right) - B_{xF}\left(\dot{\Delta}_{ixF}\right), \quad \Delta_{ixF} = x_{iF} - x_{iF0}, \quad \dot{\Delta}_{ixF} = \dot{x}_{iF} - \dot{x}_{iF0} \tag{19}$$

$$f_{iyF} = -K_{yF}\left(\Delta_{iyF}\right) - B_{yF}\left(\dot{\Delta}_{iyF}\right), \quad \Delta_{iyF} = y_{iF} - y_{iF0}, \quad \dot{\Delta}_{iyF} = \dot{y}_{iF} - \dot{y}_{iF0} \tag{20}$$

where x_{iF0} and y_{iF0} are the coordinates of foot i touchdown.

The parameters of these equations are given by [35]:

$$K_{xF} = 2\left(1+\mu\right) G \beta_x \sqrt{BL} \tag{21}$$

$$K_{yF} = \frac{G}{1-\mu} \beta_y \sqrt{BL} \tag{22}$$

where μ if the Poisson's ratio (whose value varies among 0.35 for soils of low saturation and 0.5 for fully saturated soils [35]), B is the width of the feet touching the ground and L the corresponding length. The values of β_x and β_y are extracted from pre-calculated tables given in [35] as functions of L/B. Finally G is the shear modulus and is calculated using the following expression:

$$G = \frac{E}{2\left(1+\mu\right)} \tag{23}$$

where E if the Young's modulus of elasticity of the soil type. The Young's modulus of elasticity of some common soil types are indicated in **Table 6** (extracted from [36]).

Concerning the values of damping (B_{xF} and B_{yF}) these can be calculated considering that the above expressions apply to a Mass-Spring-Dashpot system whose damping ratios are extracted from pre-calculated tables given in [35] as functions of b, being:

$$b = \frac{M}{\rho R^3} \tag{24}$$

Table 6 Young's moduli of different soil types

Soil Type	Young's Modulus (kNm^{-2})
Concrete	30000000
Wood	13000000
Gravel	100000 – 200000
Sand	10000 – 80000
Compact Clay	3000 – 15000
Loose Clay	500 – 3000
Peat	100 – 500

Table 7 Ground model parameters for different soil types

Soil Type	K_{xF}	B_{xF}	K_{yF}	B_{yF}
Concrete	2604304130	153097	3410398265	175196
Wood	1128531790	100781	1477839248	115328
Gravel	17362028	12500	22735988	14305
Sand	6944811	7906	9094395	9047
Compact Clay	1302152	3423	1705199	3917
Loose Clay	260430	1531	341040	1752
Peat	43405	625	56840	715

where M if the equivalent mass of the system under consideration (in our case $M_b n^{-1}$), ρ is the mass density of the soil [35] [36] and R is the radius of the feet-ground contact area. For the typical dimensions of the robot under consideration, the ground damping ratio either in the horizontal and vertical directions is $\zeta < 0.15$.

Based on the above theory, **Table 7** presents values for the ground model parameters of typical soils commonly found in nature and in the living environments.

In order to convert the parameters of this linear foot-ground interaction model (B_{xF}, B_{yF}) to the parameters of the non-linear model (B'_{xF}, B'_{yF}), described by Eqs. (10) and (11), we use the following relations:

$$-B'_{xF}\left(-\Delta_{iyFMax}\right) = -B_{xF} \tag{25}$$

$$-B'_{yF}\left(-\Delta_{iyFMax}\right)^{v} = -B_{yF} \tag{26}$$

where Δ_{iyFMax} if the maximum depth that the robot feet penetrates the ground.

References

[1] D. J. A. Manko, *General Model of Legged Locomotion on Natural Terrain*. Boston, MA: Kluwer Academic Publishers, 1992.

[2] S.-M. Song and K. J. Waldron, *Machines that Walk: The Adaptive Suspension Vehicle*. Cambridge, MA: The MIT Press, 1989.

[3] T. McGeer, "Passive dynamic walking," *International Journal of Robotics Research*, vol. 9, pp. 62–82, 1990.

[4] A. C. Smith and M. D. Berkemeier, "Passive dynamic quadrupedal walking," in *Proc. of IEEE International Conference on Robotics and Automation (ICRA '97)*, Albuquerque, New Mexico, USA, 1997, pp. 34–39.

[5] C.-R. Tsai and T.-T. Lee, "A study of fuzzy-neural force control for a quadrupedal walking machine," *Journal of Dynamic Systems, Measurement and Control*, vol. 120, pp. 124–133, 1998.

[6] M. C. Birch, R. D. Quinn, G. Hahm, S. M. Phillips, B. Drennan, A. Fife, H. Verma, and R. D. Beer, "Design of a cricket microrobot," in *Proc. of IEEE International Conference on Robotics and Automation (ICRA '00)*, USA, 2000, pp. 1109–1114.

[7] C.-R. Tsai, T.-T. Lee, and S.-M. Song, "Fuzzy logic control of a planetary gear type walking machine leg," *Robotica*, vol. 15, pp. 533–546, 1997.

[8] J. J. Collins and S. A. Richmond, "Hard-wired central pattern generators for quadrupedal locomotion," *Biological Cybernetics*, vol. 71, pp. 375–385, 1994.

[9] C. Zhifeng, Z. Xiuli, Z. Haojun, and Z. Liyao, "The CPG-based bionic quadruped system," in *Proc. of the IEEE International Conference on Systems, Man and Cybernetics (SMC '03)*, Washington, USA, October 2003, pp. 1828–1833.

[10] D. Wettergreen, "Robotic walking in natural terrain—Gait planning and behavior-based control for statically-stable walking robots," Ph.D. thesis, The Robotics Institute, Carnegie Mellon University, December 1995.

[11] E. Celaya and J. Porta, "Force-based control of a six-legged robot on abrupt terrain using the subsumption architecture," in *Proc. of the International Conference on Advanced Robotics (ICAR '95)*, 1995, pp. 413–419.

[12] H. J. Chiel, R. D. Beer, R. D. Quinn, and K. S. Espenschied, "Robustness of a distributed neural network controller for locomotion in a hexapod robot," *IEEE Trans. on Robotics and Automation*, vol. 8, pp. 293–303, 1992.

[13] C. Ferrell, "A comparison of three insect inspired locomotion controllers," *Robotics and Autonomous Systems*, vol. 16, pp. 135–159, 1995.

[14] F. Pfeiffer, J. Eltze, and H. Weidemann, "The TUM-walking machine (extended)," *Intelligent Automation and Soft Computing*, vol. 1, pp. 307–323, 1995.

[15] G. Nelson and R. Quinn, "Posture control of a cockroach-like robot," *IEEE Control Systems Magazine*, vol. 19, pp. 9–14, 1999.

[16] L. de S. Martins-Filho, J. L. Silvino, P. Resende, and T. C. Assunção, "Control of robotic leg joints—Comparing PD and sliding mode approaches," in *Proc. of 6th International Conference on Climbing and Walking Robots (CLAWAR '03)*, Catania, Italy, 2003, pp. 147–153.

[17] K.-P. Lee, T.-W. Koo, and Y.-S. Yoon, "Real-time dynamic simulation of quadruped using modified velocity transformation," in *Proc. of the IEEE International Conference on Robotics and Automation (ICRA '98)*, 1998, pp. 1701–1706.

[18] J. Song, K. H. Low, and W. Guo, "A simplified hybrid force/position controller method for the walking robots," *Robotica*, vol. 17, pp. 583–589, 1999.

[19] M. F. Silva, J. A. T. Machado, and A. M. Lopes, "Comparison of fractional and integer order control of an hexapod robot," in *Proc. of ASME International 19th Biennial Conference on Mechanical Vibration and Noise (VIB '03)*, ASME, Chicago, Illinois, USA, September 2003.

[20] J. A. T. Machado and A. M. S. F. Galhano, "Evaluation of manipulator direct dynamics using customized Runge-Kutta methods," *SAMS—Journal Systems Analysis-Modelling-Simulation*, vol. 17, pp. 229–239, 1995.

[21] D. W. Marhefka and D. E. Orin, "Simulation of contact using a nonlinear damping model," in *Proc. of the IEEE International Conference on Robotics and Automation (ICRA '96)*, 1996, pp. 1662–1668.

[22] K. H. Hunt and F. R. E. Crossley, "Coefficient of restitution interpreted as damping in vibroimpact," *ASME Journal of Applied Mechanics*, pp. 440–445, June 1975.

[23] M. F. Silva, J. A. T. Machado, and A. M. Lopes, "Power analysis of multi-legged locomotion systems," in *Proc. of 4th International Symposium on Climbing and Walking Robots (CLAWAR '01)*, Karlsruhe, Germany, 2001, pp. 143–150.

[24] M. F. Silva, J. A. T. Machado, and A. M. Lopes, "Performance analysis of multi-legged locomotion systems," in *Proc. of IEEE International Conference on Robotics and Automation (ICRA '02)*, Washington, D. C., USA, May 2002, pp. 2234–2239.

[25] M. F. Silva, J. A. T. Machado, and A. M. Lopes, "Power analysis of multi-legged systems," in *Proc. of 15th IFAC World Congress on Automatic Control (b '02)*, Barcelona, Spain, 2002.

[26] M. F. Silva, J. A. T. Machado, and A. M. Lopes, "Quasi-periodic gaits in multi-legged robots," in *Proc. of 5th International Conference on Climbing and Walking Robots (CLAWAR '02)*, Paris, France, 2002, pp. 733–740.

[27] P. G. de Santos and M. A. Jiménez, "Generation of discontinuous gaits for quadruped walking vehicles," *SAMS—Journal Systems Analysis-Modelling-Simulation*, vol. 12, no. 9, pp. 599–611, September 1995.

[28] M. A. Jiménez and P. G. de Santos, "Terrain-adaptive gait for walking machines," *The International Journal of Robotics Research*, vol. 16, no. 3, pp. 320–339, June 1997.

[29] S. Bai, K. H. Low, and T. Zielinska, "Quadruped free gait genera-

tion for straight-line and circular trajectories," *Advanced Robotics*, vol. 13, no. 5, pp. 513–518, 1999.

[30] Y. Y. Yi, "Locomotion of a biped robot with compliant ankle joints," in *Proc. of IEEE International Conference on Robotics and Automation (ICRA '97)*, Albuquerque, New Mexico, USA, May 2002, pp. 199–204.

[31] P. Neuhaus and H. Kazerooni, "Design and control of human assisted walking robot," in *Proc. of IEEE International Conference on Robotics and Automation (ICRA '00)*, USA, 2000, pp. 563–569.

[32] R. C. Luo, S. H. H. Phang, and K. L. Su, "Multilevel multisensor based decision function for intelligent animal robo," in *Proc. of IEEE International Conference on Robotics and Automation (ICRA '01)*, Leuven, Belgium, 2001, pp. 4226–4231.

[33] F. Zonfrilli, G. Oriolo, and D. Nardi, "A biped locomotion strategy for the quadruped robot Sony ERS-210," in *Proc. of IEEE International Conference on Robotics and Automation (ICRA '02)*, Washington, D. C., USA, May 2002, pp. 2768–2774.

[34] M. G. Bekker, *Introduction to Terrain-Vehicle Systems*. Ann Arbor, MI: University of Michigan Press, 1969.

[35] T. W. Lambe and R. V. Whitman, *Soil Mechanics, SI Version*. New York, NY: John Wiley & Sons, 1969, pp. 227 – 232.

[36] A. Suvinen, M. Saarilahti, and T. Tokola, "Terrain mobility model and determination of optimal off-road route," in *Proc. of the 9th Scandinavian Research Conference on Geographical Information Science (ScanGIS'2003)*, Espoo, Finland, June 2003, pp. 251–259.

Biographies

Manuel F. Silva was born in April 11, 1970. He graduated and received the M.S. degree in electrical and computer engineering from the Faculty of Engineering of the University of Porto, Portugal, in 1993 and 1997, respectively. Presently he is Assistant Professor at the Institute of Engineering of the Polytechnic Institute of Porto, Department of Electrical Engineering. His research focuses on multi-legged walking robots.

J. A. Tenreiro Machado was born in October 6, 1957. He graduated and received the Ph.D. degree in electrical and computer engineering from the Faculty of Engineering of the University of Porto, Portugal, in 1980 and 1989, respectively. Presently he is Coordinator Professor at the Institute of Engineering of the Polytechnic Institute of Porto, Department of Electrical Engineering. His main research interests are robotics, modeling, control, genetic algorithms, fractional-order systems and intelligent transportation systems.

António M. Lopes received a Master's degree in electrical engineering and a doctoral degree in mechanical engineering both from the Porto University in Portugal in the years 1995 and 2000, respectively. His research interests include robot modeling and control, force-impedance control and non-linear control systems.